Powder Technology 366 (2020) 185–196

Contents lists available at ScienceDirect

Powder Technology

journal homepage: www.elsevier.com/locate/powtec

Hybrid phenomenological/ANN-PSO modelling of a deformable material in spouted bed drying process

Yago Matheus da Silva Veloso [a], Marcello Maia de Almeida [b], Odelsia Leonor Sanchez de Alsina [a,c,*], Maria Laura Passos [d], Arun S. Mujumdar [e], Manuela Souza Leite [a,c,*]

[a] Post-graduate in Process Engineering, Tiradentes University, Aracaju, Sergipe, Brazil
[b] Department of Environmental and Sanitary Engineering, State University of Paraiba, Campina Grande, Paraíba, Brazil
[c] Institute of Technology and Research, Tiradentes University, Aracaju, Sergipe, Brazil
[d] Federal Univesity of Minas Gerais, Belo Horizonte, Brazil
[e] Department of Bioresource Engineering, McGill University, Montreal, Quebec, Canada

ARTICLE INFO

Article history:
Received 29 November 2018
Received in revised form 14 November 2019
Accepted 20 December 2019
Available online 24 December 2019

Keywords:
Guava
Spouted bed
Physical properties
Neural network
Hybrid model

ABSTRACT

In this work, a hybrid (phenomenological/ANN-PSO) model has been developed to simulate the spouted bed drying of deformable solid materials, considering material shrinkage and the physical property variation during drying. Accordingly, an artificial neural network (ANN) model has been coupled to a phenomenological one to describe the heat and mass transfer during the drying of these materials, specifically of guava pieces, in a spouted bed dryer. The optimum architecture of ANN (4–7-3) has been obtained using a Particle Swarm Optimisation (PSO) algorithm. This model demonstrated higher accuracy in its ability to estimate the material physical properties ($R^2 = 0.99$, MSE = 0.00048 and RMSE = 0.069). Furthermore, a comparison between the model results and experimental data provided high correlation. This differs from the usual approach, which neglects variation of the physical properties; the hybrid model is able to simulate the drying deformable particle process behaviour considering the transient variation of the properties obtained from the ANN-PSO model. The results differ significantly from those predicted with the assumption of constant properties.

1. Introduction

Drying is the most common preservation method applied widely to produce dried fruits and vegetables. This is because it retards their deterioration due to microbial activity, by removing water from them without causing significant physical, nutritional and sensory loss [1,2], if drying is carried out under appropriate operating conditions. This technique is an effective way to reduce perishability and increase the shelf life of products at a reasonable cost. Specifically for guava pieces, the drying temperature should be <70 °C to avoid thermal degradation.

Recently, spouted bed (SB) technology has been used to dry coarse particles ($d_p > 1$ mm) because it provides a high solid circulation rate and, consequently, effective contact between the drying agent and the solid particles [3,4] leading to high heat and mass transfer rates. This drying technique is widely used for the drying of numerous products, including suspensions [5], pastes [6,7], seeds [8,9], fruits [10–12], and vegetables [13]. It should be noted that not all materials can be spouted and hence this application is limited to only spoutable materials.

Although Geldart type D particles can be spouted stably, the problem generated in SB dryers of deformable and shrinkable materials is the solid-fluid flow instability due to changes in the material properties during drying. This affects the spouting operation, the solid-fluid contact and the mass and heat transfer. Almeida et al. [10] have presented and discussed the flow regime maps obtained during the drying of diced guava in an SB, corroborating the fact that the flow stability in this dryer is function of the air flow rate and the moisture content variation. Therefore, one strategy to maintain this stability at spout-fluid and spouting regimes is to control operational variables such as the air velocity and temperature during SB operation [10]. If the drying material properties change during drying, it is necessary to modify them for optimal spouting conditions. Thus, a time-real control system must be developed to avoid the flow instability in such SB dryers of deformable and shrinkable materials, requiring appropriate models to simulate the drying process which can respond promptly at a prescribed time within defined time tolerances.

Several studies in the literature present models for particle drying in spouted and fixed beds [1,14,15]. Some of these models incorporate deformable particles drying in a spouted bed, such as guava pieces, carrot

* Corresponding authors at: Institute of Technology and Research, Tiradentes University, Av. Murilo Dantas 300, Farolândia, Aracaju 49032-490, Sergipe, Brazil.
E-mail addresses: odelsia@uol.com (O.L.S. de Alsina), manuela_leite@itp.org.br (M.S. Leite).

https://doi.org/10.1016/j.powtec.2019.12.047
0032-5910/

Nomenclature

a_e	specific area of the solid in contact with drying air (m^2. m^{-3})
C_p	specific heat capacity of the particle (J. kg^{-1}. K^{-1})
$C_{p\ air}$	specific heat capacity of the air (J. kg^{-1}. K^{-1})
d	diameter (m)
E_{val}	validation error
E_{opt}	optimisation error
g	acceleration of gravity ($m.s^{-2}$),
G	drying air mass flow ($kg.s^{-1}$)
h	heat transfer coefficient between the dryer wall and the external air ($W.m^{-2}$ K^{-1})
h_p	heat transfer coefficient between the air drying and particle bed ($W.m^{-2}$ K^{-1})
h_w	heat transfer coefficient between the particle bed and the dryer wall ($W.m^{-2}$ K^{-1})
H	enthalpy of moist air ($J.kg^{-1}$)
H_i	initial bed height (m)
k	thermal conductivity ($W.m^{-1}$. K^{-1})
L	dryer height (m)
m	mass of solids (kg)
MC	moisture content (−)
Nu	Nusselt number ($h_p\ d_p/\ k_{air}$) (−)
Pr	Prandtl number ($c_p\ \mu/\ k$) (−)
Q	loss heat (W)
Ra	Rayleight number ($g\ \beta\ \Delta T\ L^3/\ \nu\ \alpha$) (−)
Re	Reynolds number ($d_p\ \rho_{air}\ u/\ \mu_{air}$) (−)
t	time (s)
T	temperature (K)
u	superficial air velocity ($m.s^{-1}$)
u_{air}	operational air velocity ($m.s^{-1}$)
$u_i^{\rightarrow}(t)$	position vector of particles in PSO algorithm
V_b	volume of the bed of particles (m^3)
$v_i^{\rightarrow}(t)$	velocity vector of particles in PSO algorithm
W	absolute humidity of air ($kg_{\ water\ vapor}.\ kg^{-1}_{\ dry\ air}$)

Greek symbols

λ	latent heat of vaporisation (J. Kg^{-1})
ρ	density ($kg.m^{-3}$)
μ	viscosity ($kg.m^{-1}.s^{-1}$)
β	thermal expansion coefficient (K^{-1})
ν	kinematic viscosity ($m^2.s^{-1}$)
α	thermal diffusivity ($m^2.s^{-1}$)

Subscripts

amb	ambient air
air	drying air
d.b	dry basis
ds	dry solid
ext.	external
i	initial
in	inlet
int	internal
opt	optimisation step
out	outlet
p	particle
val	validation step
wall	dryer wall

cubes and shrimp [10,13,15]. However, mathematical models based on physical phenomena are difficult to solve due to their high nonlinearity and the coupled effects of various operational and physical variables in spouted beds [2]. Such difficulty results in increasing computer resolution time and reduces their use in controlling processes.

An artificial neural network (ANN) model based on the mode of learning of the biological neurons of the human brain is now recognised as an important tool for modelling complex nonlinear and dynamic systems. Particularly for applications in which conventional modelling approaches fail [2]. ANN models are widely used in various fields of science and engineering [16–19]. In drying applications, such models have been used for pattern recognition and classification [20–22] and for predicting the physical properties of materials during drying [12,23–25]. A comprehensive review of the ANN applications [2] summarises the use of this approach in modelling various dehydration methods, including SB drying. Moreover, it is recommended that the ANN model be used as a complement to existing mathematical models rather than as an alternative [2].

Another alternative to the use of the stand-alone ANN approach is to couple it with a phenomenological model to estimate and adjust the process parameters, thus resulting in a hybrid model [7]. Some studies in the literature have reported the use of hybrid models applied to drying processes for several materials [7,26]. In [7] a hybrid model based on the global balance of mass and energy and a phase-coupling term given by a neural network was proposed in order to describe milk drying in spouted bed. The proposed models presented good results under the conditions in which the spouting behaved as a perfectly stirred tank for the estimates of pressure drop and of the behaviour of heat and mass transfer phenomena. The use of a hybrid CSTR/neural network model to describe the highly coupled heat and mass transfer during paste drying with inert particles in vibrofluidized beds was proposed by [26].The dynamics behaviour of the outlet air temperature and relative humidity were well described by the CSTR lumped model for most conditions evaluated.

Previous experimental studies of SB drying of pieces of guava investigated the behaviour of physical properties of this material and the fluid dynamics during drying to study the phenomenon of shrinkage [10]. In the present paper, a hybrid (phenomenological/ANN-PSO) model is proposed and developed to predict the drying of deformable particles in SBs, including changes in the properties of spouting air and guava pieces during drying. This allows a more realistic model to be used in the process control, which requires an accurate output variable response at a prompt time. Note that these changes in solid-fluid properties are essential to the further development of control systems to maintain the stability of SB.

2. Materials and methods

2.1. Materials and drying equipment

Guavas of the "Paluma" variety, acquired in the market of Campina Grande, Brazil, were chosen after checking them visually, for physical damage, colour and consistency. The SB dryer used in this study has a height of 1 m and a conical base with an included angle of 60 degrees and a height of 0.09 m. The internal cylindrical diameter and the spouting nozzle orifice diameter are 0.108 m and 0.028 m, respectively. All experiments carried out in this SB dryer follow the experimental design shown in Table 1. In Table 1, H_i is the initial height of the static bed, $M.C_{i\ (d.b)}$ is the initial moisture content on dry basis of the pieces of guava and u_{air} is the inlet spouting air velocity. These input (or independent) variables as well as their experimental levels have been defined on the basis of the fluid dynamic model developed for the SB of guava pieces in an earlier work [10].

2.2. Experimental procedure

Diced guava pieces were partially dried in a fixed bed to adjust the moisture content level to the range of the experimental design (0.6; 1.05 and 1.5 expressed in dry basis). Although this moisture content

Table 1
Experimental design for the spouted bed drying tests.

Run	Input variables		
	H_i (m)	$M.C_{i\ (d.b)}$	u_{air} ($m.s^{-1}$)
1	0.09	0.6	2.8
2	0.12	0.6	2.8
3	0.09	1.5	2.8
4	0.12	1.5	2.8
5	0.09	0.6	3.5
6	0.12	0.6	3.5
7	0.09	1.5	3.5
8	0.12	1.5	3.5
9	0.105	1.05	3.2
10	0.105	1.05	3.2

range allows the SB of guava pieces to reach the spouting regime, the spouting instability occurs in most of the designed tests in Table 1. This is a behaviour that is typical of group C in the Geldart classification [27].

During the drying tests, it has been observed that the guava pieces tend to round their corners quickly enough to approach their shape to a sphere. Therefore, the particle size of guava pieces can be characterised by the equivalent particle diameter of the sphere with the same particle volume, d_p. Based on the particle volume measurement, the initial d_p is 7.9 mm for $MC_i = 0.6$ and 8.6 mm for $MC_i = 1.5$, and a variation in d_p of 2 mm has been observed at the end of the drying operation.

For each test performed, guava samples of 2 g were taken from the SB dryer at regular time intervals to measure their properties (density, moisture content and diameter). Since the guava sample presented a high degree of deterioration at temperatures above 70 °C, the moisture content was determined by the oven method at 70 °C for 24 h in the presence of silica gel. The density is determined by a liquid pycnometer using ethanol and the particle diameter calculated by the sphere with the same volume as the particle. The removal of guava piece samples from the drier was performed carefully to ensure that the solids loading inside the drier and the drying kinetics were not significantly changed.

2.3. Artificial neural network model development

The ANN model to predict the physical properties of guava pieces has been developed using the software Matlab 4.0 (Neural Network Toolbox), consisting of the selection of the model architecture, training, and validation, and testing of the generated algorithm.

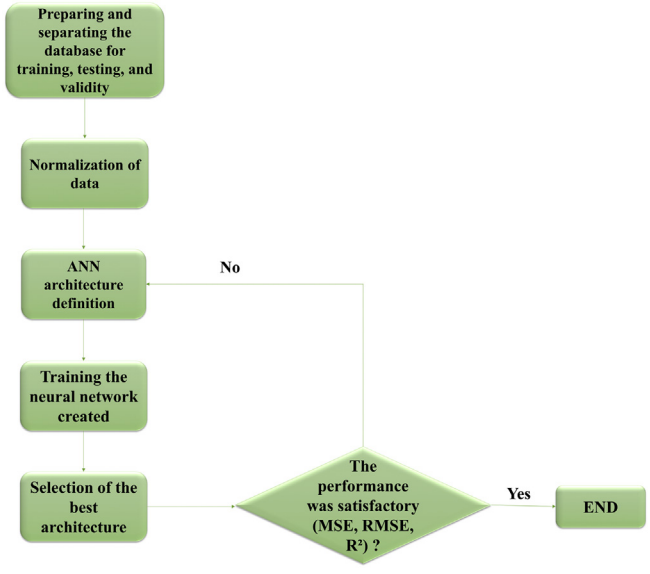

Fig. 1. Flowchart of ANN based model construction [29].

The feed-forward back propagation neural network was used to create the ANN model for mapping layers of input (independent) and output (desired response) variables. This ANN model type was selected for presenting good applications in non-linear systems [18,25,28]. The adjustment of the neural parameters (synaptic weights) during development model was achieved by the Back propagation Levenberg-Marquardt algorithm.

The first step was to select the network architecture that best fit the data, so that the results produced by the network were the closest to the experimental data. In this step, the number of hidden layers, the number of neurons in the hidden layer, the activation functions and the training algorithms are defined.

For ANN training, validation and testing, the criteria used were the Mean Squared Error (MSE), the Root Mean Squared Error (RMSE) and the determination coefficient (R^2) to evaluate the performance of the model. The steps employed to create the ANN models are described in the flowchart (Fig. 1).

2.3.1. Data processing

To develop the neural model, a database containing 180 samples was used. Experimental data were added at different times within the ranges tested. For this purpose, MATLAB was used with a pre-programming routine for numerical interpolation. This increase in the number of samples in the databases was necessary to ensure that the network did not lose its ability to represent the process well. The use of numerical interpolation [30] and the standard deviation technique [31] to increase the number of samples in the database has been reported in the literature to enhance the reliability of ANN models.

The databases were randomly arranged to prevent the neural network model from being concentrated in a certain experimental range of the process and separated into three databases: training (70%), validation (15%) and test (15%). The databases were composed by the results of the 10 experimental runs contained in Table 1.

The databases were normalised between values of −1 and + 1 using the maximum and minimum values of each variable contained in the databases according to Eq. (1). This normalisation was necessary to avoid the tendency for the network to have a greater consideration of values of greater magnitude in databases.

$$y = (y_{max} - y_{min})\,(x - x_{min})/(x_{max} - x_{min}) + y_{min} \quad (1)$$

In Eq. (1), y_{max} is equal to 1, y_{min} is equal to −1, x_{max} is the maximum value the variable assumes and x is the value of the variable being normalised.

2.3.2. Architecture model definition

In this step, the number of the hidden layer, the number of neurons used in the hidden layer, the activation functions and the training algorithm were defined. In neural network Back Propagation training, the learning algorithm has a tendency to show problems of slow convergence and to get trapped in local minima. Particle swarm optimisation algorithms have been recognised as the most efficient training algorithms as they avoid getting trapped at local minima, and, more interestingly, these have fast convergence rates [32–35].

To reduce the number of tests needed to fit the parameters of the model, a methodology for optimisation of the parameters based on the "Particle Swarm Optimisation" (PSO) algorithm was employed. This search algorithm is based by the social and collective habits of birds flocking and fish schooling [32]. In PSO algorithms, a system is initialised with a population of particles and a subset of these particles represent the potential solution. This algorithm starts to research the optimal point in the hyperspace of possible solutions. Iteration by iteration, the particles of the swarm learn with their experience and also the best experience of the particle group. The best position of each particle is named personal best and the overall best position of particles in the swarm is named the global best. At each iteration, each particle tends

to move towards the direction of the personal and global best position [32,33].

Fig. 2 shows the flowchart used to optimise the ANN using the PSO algorithm. First, the PSO randomly initialised the particles containing a number of neurons, the activation function and learning rate, as well as the position and velocity of each particle, which is updated at each iteration. The algorithm starts searching for the optimal solution within the hyperspace of potential solutions. The particles learn at each iteration to respond appropriately based on the "experience" of other particles.

The number of dimensions in the problem space is equal to the number of components there are to optimise. If, $x_i^{\rightarrow}$ and $v_i^{\rightarrow}$ represent position and velocity vector, a particle updates its position according to the Euler integration equation for physical movement given as [32]:

$$x_i^{\rightarrow}(t) = x_i^{\rightarrow}(t-1) + v_i^{\rightarrow}(t) \tag{2}$$

Training, validation and tests of the ANN model

In the training step, different numbers of neurons, learning rates and activation functions between the input layer and intermediate layers were tested: e.g. linear, hyperbolic tangent and logarithmic sigmoid according to Eqs. 3, 4 and 5, respectively. Here, n is the input value, a is the slope parameter of the logarithmic sigmoid function and $y_{(n)}$ is the output of the neuron.

$$y(n) = n \tag{3}$$

$$y(n) = \left(2/\left(1 + e^{-2n}\right)\right) - 1 \tag{4}$$

$$y(n) = 1/\left(1 + e^{-an}\right) \tag{5}$$

The early-stopping rule based on cross-validation was used as the stop criterion. Cross validation can be used to detect when over-fitting starts during the supervised training of a neural network; training is then stopped before convergence to avoid the over-fitting ("early stopping"). This phenomenon refers to the reduction in generalisation ability that can occur as networks are trained, and must be avoided [36,37]. The ANN was trained on a Matlab platform version R2016a, it was used

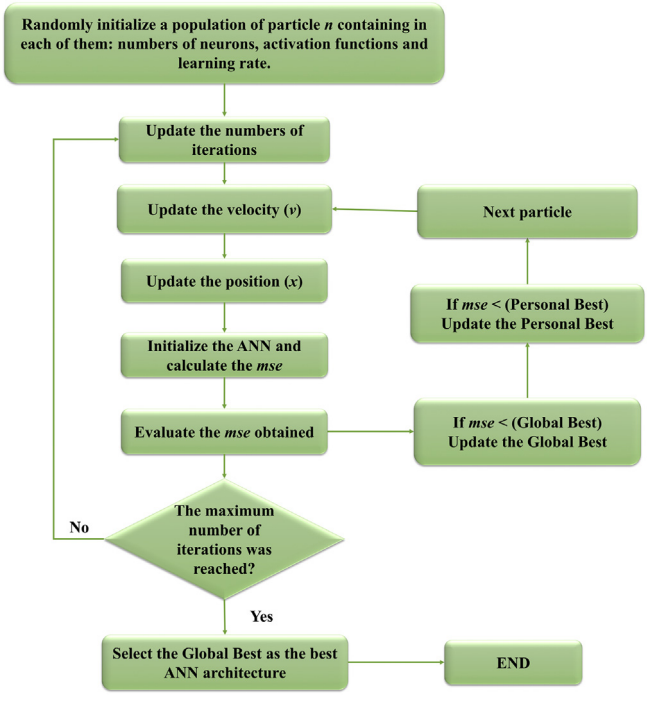

Fig. 2. Flowchart of PSO algorithm to optimise the ANN architecture [33].

a computer equipped with a 2.3 GHz power processor and 8 GB of RAM memory. The total iteration number was set at 3000 for all training algorithms and the performance goal is set at 10^{-7}, the model simulation and training require low computational time.

The objective function (error function) of the training algorithm, is the squared error. $E_{val}(t)$ is the corresponding error in the validation set and is used by the stopping criterion. The value $E_{opt}(t)$ is defined to be the lowest validation set error obtained in epochs up to t (Eq. 6).

$$E_{opt} = min_{t^{\ddot{E}} \le t} E_{val}\left(t^{\ddot{E}}\right) \tag{6}$$

The stopped criteria decide to stop at some time t during training and the result of the training is then the set of weights that exhibited the lowest validation error $E_{op}(t)$.

The test model generates MSE (Eq. 7), RMSE (Eq. 8) and R^2 (Eq. (9)) values.

$$MSE = \sum \left(y_{i\ calc} - y_{i\ \ exp}\right)^2 / n \tag{7}$$

$$RMSE = \sqrt{\sum \left(y_{i\ calc} - y_{i\ \ exp}\right)^2 / n} \tag{8}$$

$$R^2 = \sum \left(y_{i\ calc} - \overline{y}\right)^2 / \sum \left(y_{i\ \ exp} - \overline{y}\right)^2 \tag{9}$$

Here, $y_{i\ exp}$ is the real value, obtained via experiments, $y_{i\ calc}$ is the value produced by the neural model, $\overline{y}$ is the average value of the samples and n is the number of experimental samples.

2.4. Hybrid model development

To describe the heat and mass transfer phenomena in the SB drying of guava pieces, the global heat and mass balance equations have been derived based on the following assumptions:

- Guava pieces are spherical particles and undergo shrinkage during drying;
- The height of the annulus region is equal to the height of the static bed, neglecting the effects of expansion and/or shrinkage;
- The temperature and moisture content gradients inside the particle are neglected, meaning that the particle temperature and moisture content vary only with the drying time;
- In calculating the heat transfer coefficient between particle and air (h_p), the heat transfer contributions of the spout and fountain region were neglected. According to Uemaki and kugo [38], the whole area of particules was used.

Based on these assumptions, the global mass and energy balances can be described by Eqs. (10) and (11):

$$G\left(H_{in} - H_{out}\right) = h_p\, a_e\, \Delta T\, V_b + Q \tag{10}$$

$$m_{ds}\, d\left(M.C_p\right)/dt = G\left(W_{in} - W_{out}\right) \tag{11}$$

The particle temperature variation and the outlet air temperature in the dryer is obtained from energy balance according to Eqs. 12 and 13.

$$m_{ds}\, \lambda\, d\left(MC_p\right)/dt + C_p\, m_{ds}\, dT_p/dt = h_p\, a_e\, \Delta T\, V_b \tag{12}$$

$$\Delta T = \left(\left(T_{air,in} - T_p\right) + \left(T_{air,out} - T_p\right)\right)/2 \tag{13}$$

2.4.1. Heat transfer coefficient between the drying air and particle bed

To estimate the global heat transfer coefficient between the drying air and the particle in a fixed bed (h_p), Eqs. (14)–(17) were used [38]. To estimate the global heat transfer coefficient between the drying air

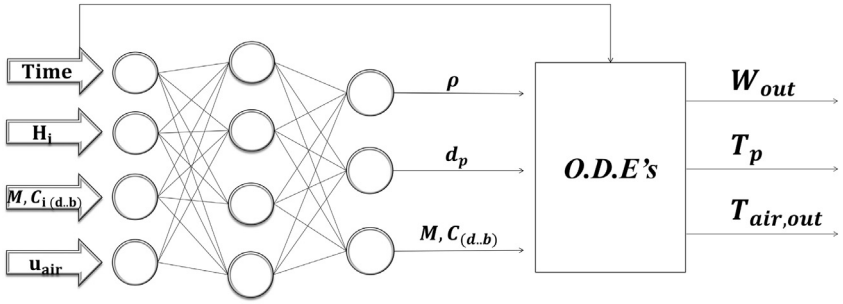

Fig. 3. Flow diagram of the data for the process to the numerical solution of the hybrid model.

and the particle in a spouted bed (hp), Eqs. (14)–(17) were used [38]. The correlation of Uemaki and Kugo, Eq. (14), was obtained through experimental conditions, Reynolds range and bed geometry similar to those of the present work.

$$Nu = 0,0005\ \ \mathrm{Re}^{1.46}\ (\mathrm{u/ums})^{1.3} \tag{14}$$

$$Nu = \mathrm{hp.dp/kair} \tag{15}$$

$$\mathrm{u} = \mathrm{G}/\rho\mathrm{airAcol} \tag{16}$$

$$\mathrm{Rep} = \mathrm{d_p}\ \rho_{air}\ \mathrm{u_{ms}}/\mu_{air} \tag{17}$$

2.4.2. Heat transfer coefficient between the particle bed and dryer wall

The heat transfer coefficient of the particle bed to the dryer wall was estimated by Eq. 18, applied for $\mathrm{Re_p} > 4$ [39,40]. This $\mathrm{Re_p}$ condition is certified for all experiments carried out in this work.

$$\mathrm{h_w} = 0.6\ (\mathrm{u\ d_p}\ \rho_{air}/\mu_{air})^{0.39}\ (\mathrm{C_{p\ air}}\ \mu_{air}/\mathrm{k_{air}})^{0.72}\ (\rho_p\ \mathrm{C_p}/\rho_{air}\ \mathrm{C_{p\ air}})^{0.12}\ (\mathrm{k_{air}}/\mathrm{d_p}) \tag{18}$$

2.4.3. Heat transfer coefficient between the dryer wall and ambient air

Heat transfer to the ambient air from the dryer wall has been determined by the correlation for thermal exchange in the vertical cylinders proposed by Churchill & Chu [40]. This correlation, expressed by Eqs. (19)–(21), has been used to determine the heat transfer coefficient, h, between the dryer wall and ambient air.

$$Nu = \left(\left(0.825 + 0.387\ \mathrm{Ra}^{1/6}\right)/\left(1 + (0.492/\ Pr)^{9/16}\right)^{8/27}\right)^2 \tag{19}$$

$$Ra = \left(\mathrm{g}\ \beta\ (\mathrm{T_{wall}}-\mathrm{T_{amb}})\ \mathrm{L}^3\right)/\nu\ \alpha \tag{20}$$

$$\mathrm{h} = Nu\ \mathrm{k_{air}}/\mathrm{L} \tag{21}$$

2.4.4. Estimation of heat loss

The heat loss through the dryer wall to the air ambient was calculated by Eq. (22). The range of calculated heat loss during drying was 0 ($t = 0$) to 41.8 W ($t = 3600$ s).

$$\mathrm{Q} = (\mathrm{T_{air,out}}-\mathrm{T_{amb}})/(1/\mathrm{h_p}\ 2\pi\ \mathrm{r_{int}}\ \mathrm{H_i}) + (\ \ln(\mathrm{r_{ext}}/\mathrm{r_{int}})/2\pi\ \mathrm{k_{wall}}\ \mathrm{L}) + (1/\mathrm{h}\ 2\pi\ \mathrm{r_{ext}}\ \mathrm{L}) \tag{22}$$

2.4.5. Numerical solution for the hybrid model

Measurements of particle properties during drying in SB are unreliable due to disturbances such measures could introduce into the system compromising accuracy [7,39]. Thus, estimation of variables using a phenomenological model based on such measurements is often difficult but empirical or semi-empirical models (e.g. artificial neural networks) can be used as a parameter estimator. It yields grey-box neural models or a hybrid model that can be a good alternative to modelling complex phenomena [6,7,41]. This is the case of drying deformable particles in a spouted bed dryer, which entails variable properties during drying.

During the drying of diced pieces of guava, abrupt variations in physical properties were observed as a function of the moisture content and volumetric shrinkage. Therefore, this cannot be neglected in calculations of the phenomenological model for heat, mass and momentum balance transfer. It is practical to use the ANN model to predict the particle physical properties (ρ, $\mathrm{d_p}$ and $\mathrm{M.C_{(d.b)}}$) during drying, thus forming a hybrid model. Fig. 3 shows a flow diagram of the data needed in the process to solve the ordinary differential equations (ODEs) (Eqs. (9) and (10)) of the hybrid model.

Through solution of the hybrid model, the particle temperature profiles ($\mathrm{T_p}$) and the outlet air temperature ($\mathrm{T_{air,\ out}}$), as well as the outlet air humidity ($\mathrm{W_{out}}$), are computed. The ODEs described in Fig. 3 have been solved numerically by the finite difference method implemented in the MATLAB code. The initial conditions applied are: $\mathrm{M.C_{(0)}} = \mathrm{M.C_{(0),\ exp}}$ and $\mathrm{Tp_{(0)}} = \mathrm{Tp_{(0),\ exp}}$. at $t = 0$.

3. Results and discussion

3.1. Physical property modelling using ANN-PSO model

The experimental data, e. g. processing time, initial moisture content on dry basis ($\mathrm{M.C_{i\ (d.b)}}$), spouting air velocity ($\mathrm{u_{air}}$) and the initial bed height ($\mathrm{H_i}$) were selected as the input variables of the ANN model. Density (ρ), particle diameter ($\mathrm{d_p}$) and moisture content on dry basis ($\mathrm{M.C_{(d.b)}}$) were chosen as the output variables.

Although ANN fitting is purely empirical and does not provide any physical insight, it is very useful in the case of deformable materials, because ANN can be used as a tool to predict density, particle diameter and moisture content variations during drying. From this information incorporated into the hybrid model, more realistic results are expected, especially for process control purposes.

The ranges of the input and output variables of the model are listed in Table 2.

Table 2
Ranges of input and output variables of the ANN model.

Variables	Range
Input	
Time (min)	0–60
$\mathrm{u_{air}}$ ($\mathrm{m.s^{-1}}$)	2.8–3.5
$\mathrm{H_i}$ (m)	0.09–0.12
$\mathrm{M.C_{i\ (d.b)}}$	0.60–1.5
Output	
ρ ($\mathrm{kg.m^{-3}}$)	893.4–1113.4
$\mathrm{d_p}$ (m)	0.0063–0.0086
$\mathrm{M.C_{(d.b)}}$	0.1082–1.5
$\mathrm{Re_p}$	943–1616

Table 3
Parameters of the ANN model architecture optimised using the PSO algorithm.

Optimised parameters	Variation
Numbers of neurons	From 1 to 9 neurons
Activation Functions tested	Linear, hyperbolic tangent and logarithmic sigmoid
Learning Rate	From 0 to 1

PSO algorithm parameters have significant effects on the optimal configuration of the ANN- PSO model. A trial-and-error procedure has been applied for tuning the PSO parameters e.g. particle personal best, particle global best and number of particles; these parameters were defined as 1.6, 1.6 and 25, respectively [33].

Table 3 shows the parameters of the neural model, as well as their range optimised by the PSO algorithm. This algorithm evaluates the network by the MSE value obtained after each training step and chooses as the best architecture of the network the one that presents the lowest value of this parameter of performance.

The ANN model has been trained using the *Levenberg-Marquardt* back-propagation algorithm. Fig. 4 shows the optimised architecture of the ANN model according to the PSO algorithm, obtained for the condition of the lowest performance index values. This optimised architecture consists of 4 neurons in the input layer, which uses a hyperbolic tangent activation function; 7 neurons in the hidden layer which use hyperbolic tangent activation function; and finally, the 3 neuron output layer which uses a linear activation function. Thus, the ANN model has final architecture 4–7-3. The optimal learning rate found to be 0.56. Learning rate is the rate at which the accumulation of information in a neural network progresses over time and it is one of the most important hyper-parameters to tune for training deep neural networks [2,23,42,43].

Table 4 shows the values of mean squared error (MSE), root mean squared error (RMSE) and correlation coefficient (R^2) to the optimised ANN model for the training, validation and testing database respectively.

Several studies in the literature reported similar results in the modelling of drying using ANN e.g. the modelling of outlet air temperature in the maltodextrin and lactose drying in spray dryer [23]. The density and porosity prediction for raspberry drying in a fixed bed [12]; and the prediction of drying kinetics of Brazilian pepper- tree fruits in a fixed bed [24].

The highest and lowest experimental values, as well as the ANN predicted values for each of the three output variables of the model are presented in Table 5.

Table 4
Performance indexes obtained by the hybrid ANN model for the training, testing and validation database.

ANN model architecture	Data base	MSE	RMSE	R^2
4–7-3	Training	0.0048	0.069	0.99
	Validation	0.0045	0.067	0.98
	Testing	0.0038	0.062	0.96

Table 5
Minimum and maximum experimental and predicted values for the three output variables.

Variables		Experimental value	ANN predicted value
ρ (kg.m^{-3})	Minimum value	893.4	890.6
	Maximum value	1113.4	1110.9
d_p (m)	Minimum value	0.0063	0.0064
	Maximum value	0.0086	0.0087
M.C $_{(d.b)}$	Minimum value	0.108	0.090
	Maximum value	1.520	1.506

Neural Networks model appear to be a predictive tool that allows accurate response of physical properties (e.g. density, particle diameter, moisture content) resulting in a relative error value under 1%.

To measure the ANN model performance during training, validation and test, and to avoid overtraining (the network being too specialised in the training set), it is common practice to monitor the behaviour of the error during each of these steps (early-stopping rule). The cross-validation stopping improves the generalisation ability of the network. It is important to note that excessive training occurs when the training error decreases while the validation error increases for a certain number of epochs [42,43].

Fig. 5 presents MSE variation as a function of the number of epochs for the model. It can be noticed that for each new iteration made by the model during training, validation and test, the respective MSE value for each step is minimised. To avoid overtraining for the developed model, the weights and biases of the model were calculated for 32 epochs, where the minimum computed value of error MSE was 0.0052.

Fig. 6 shows the correlation between the experimental data and the predicted results by ANN-PSO model for training, validation and test databases. It can be concluded that the current ANN model shows a satisfactory fit with the experimental data.

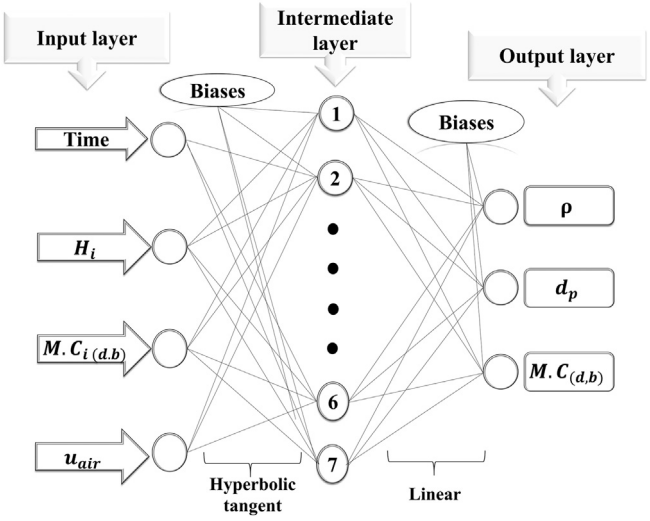

Fig. 4. Optimised architecture of the neural network model to predict the physical properties of deformable material.

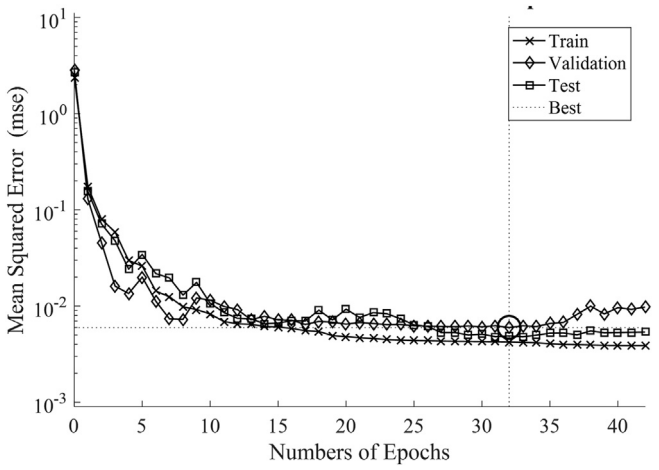

Fig. 5. Performance of the ANN-PSO model by analyses of the MSE value as a function of the number of epochs using training, validation and test databases.

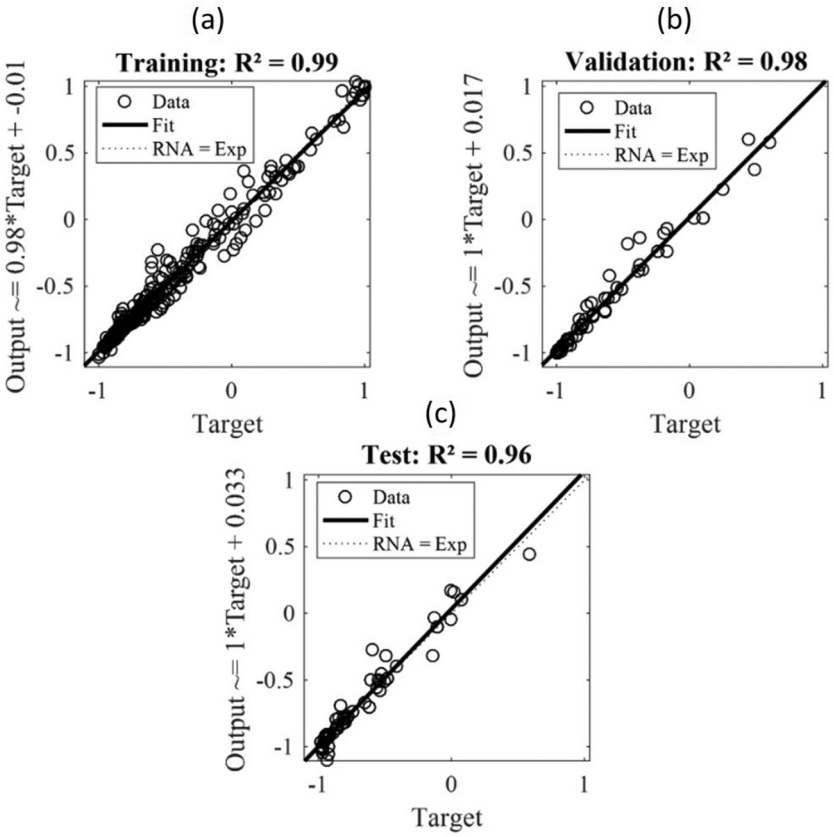

Fig. 6. Linear regression results for a) training, b)validation and c) test of the ANN-PSO model.

Table 6
Weights and biases matrix of the ANN-PSO model.

Neurons	Weights and biases between neurons at input and hidden layer					Weights and biases between neurons at hidden layer and output layer			
	Weights				Biases (B_1)	Weights			Biases (B_2)
	Time	H_i	$M.C_{i\ (d.b)}$	u_{air}		ρ	d_p	$M.C_{(d.b)}$	
1	−1.33	3.36	2.36	−1.78	2.75	0.27	0.64	0.27	1.33
2	1.73	−1.66	2.97	1.42	−2.51	−0.18	−0.42	−0.18	0.64
3	0.44	3.04	0.44	−1.10	0.67	−0.19	−0.48	−0.19	1.33
4	3.59	−0.01	−0.50	0.02	4.43	−1.85	−0.44	−1.85	
5	0.46	−4.34	−0.09	−0.01	1.42	0.04	0.08	0.04	
6	−1.29	0.22	−0.05	−0.05	−1.61	0.45	1.12	0.45	
7	0.95	−1.11	−3.45	−2.95	2.40	−0.15	−0.35	−0.15	

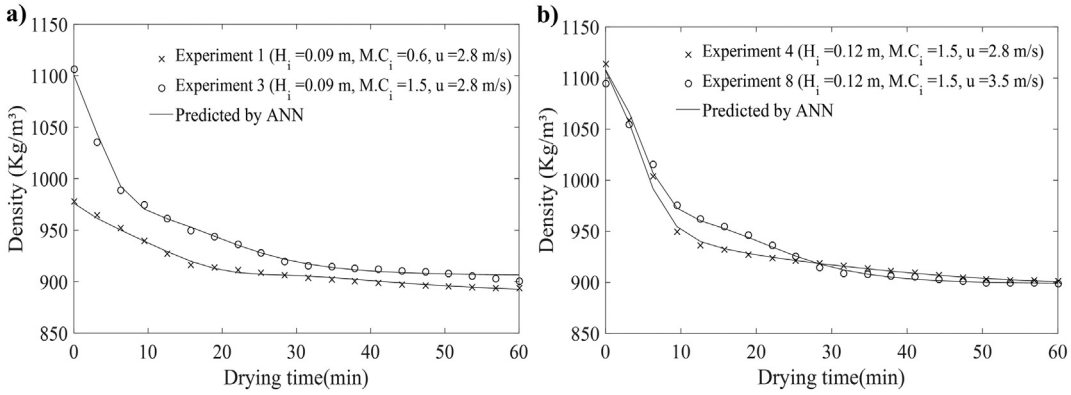

Fig. 7. Experimental and simulated variation of particle density: a) Run 1 ($H_i = 0.09$ m, $M.C_i = 0.6$ e $u_{air} = 2.8$ m.s^{-1}) and Run 3 ($H_i = 0.09$ m, $M.C_i = 1.5$ e $u_{air} = 2.8$ m.s^{-1}) and b) Run 4 ($H_i = 0.12$ m, $M.C_i = 1.5$ e $u_{air} = 2.8$ m.s^{-1}) and Run 8 ($H_i = 0.12$ m, $M.C_i = 1.5$ e $u_{air} = 3.5$ m.s^{-1}).

The weights and biases of the optimised neural net model obtained in the training step are also presented in Table 6. The output parameters of the ANN model were simulated using Eqs. (23)–(24) and (25).

$$\rho = \text{Purelin}\ \{\text{Tansig}\ (-8.1\ \text{Time} + 0.728\ H_i + 1.4\ M.C_i - 0.123\ u_{air} - 8.142) + 1.33 \quad (23)$$

$$d_p = \text{Purelin}\ \{\text{Tansig}\ (-5.12\ \text{Time} + 1.67\ H_i + 1.4\ M.C_i - 0.264\ u_{air} - 1.961) + 0.64 \quad (24)$$

$$M.C_{(d.b)} = \text{Purelin}\ \{\text{Tansig}\ (-8.1\ \text{Time} + 0.728\ H_i + 1.4\ M.C_i - 0.123\ u_{air} - 8.142) + 1.33 \quad (25)$$

3.2. Prediction of the physical properties by the neural model

After definition of the best ANN model architecture for estimating the physical properties of guava during drying in a spouted bed, network tests were carried out to verify its predictive ability under different experimental conditions. Figs. 7, 8 and 9 demonstrate the variation of physical properties (ρ, d_p e M.C $_{(d.b)}$) for different experimental conditions of H_i, $M.C_i$ and u_{air} shown in Table 1. The maximum elapsed time simulated by the model is 60 min.

It can be seen in Fig. 7a and b that the rate of reduction of particle density along the drying is influenced by the initial moisture content, being more important for higher levels of moisture. Otherwise, no significant influence of air velocity on the rate of density variation was observed.

Fig. 8 shows that the initial bed height, initial moisture content and air velocity have an influence on the variation of particle diameter during drying. Lower values of initial bed height and/or higher air velocities result in higher solid circulation rates within the bed, causing a better contact and attrition between the drying air and the solids causing greater deformation of particles. The deformation and consequent shrinkage of the materials during drying is due to the strength that affects the cellular structure of the material. These phenomena occur to a broad extent when the moisture is significant and the material is anisotropic, conditions which are found in the drying of fruits and vegetables [13,44,45].

Fig. 9a and b show that even under different experimental conditions of H_i, $M.C_{i\ (d.b)}$ and u_{air}, equilibrium moisture content was obtained for the operational time of 60 min. Drying occurs in the falling rate period, except the first 150 s at the start of the process and the rate reduces significantly after 30 min, attaining moisture values close to equilibrium, 0.16 $_{db}$.

The spouting air velocity does not have a great influence on the drying kinetics of guava pieces (Fig. 9b). A similar behaviour was observed in the drying of Brazilian pepper-tree fruits in fixed bed [24].

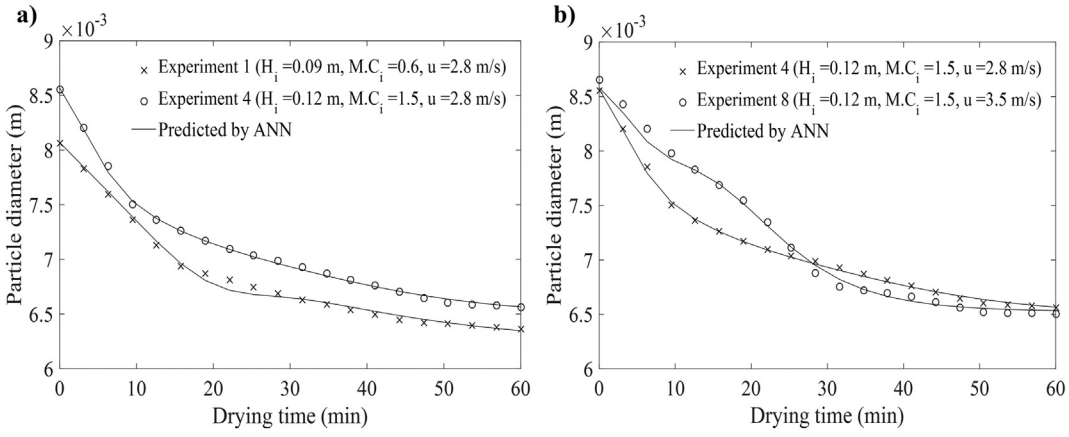

Fig. 8. Experimental and simulated variation of the particle diameter: a) Run 1 (H_i = 0.09 m, $M.C_i$ = 0.6 e u_{air} = 2.8 m.s^{-1}) and Run 3 (H_i = 0.09 m, $M.C_i$ = 1.5 e u_{air} = 2.8 m.s^{-1}) and b) Run 4 (H_i = 0.12 m, $M.C_i$ = 1.5 e u_{air} = 2.8 m.s^{-1}) and Run 8 (H_i = 0.12 m, $M.C_i$ = 1.5 e u_{air} = 3.5 m.s^{-1}).

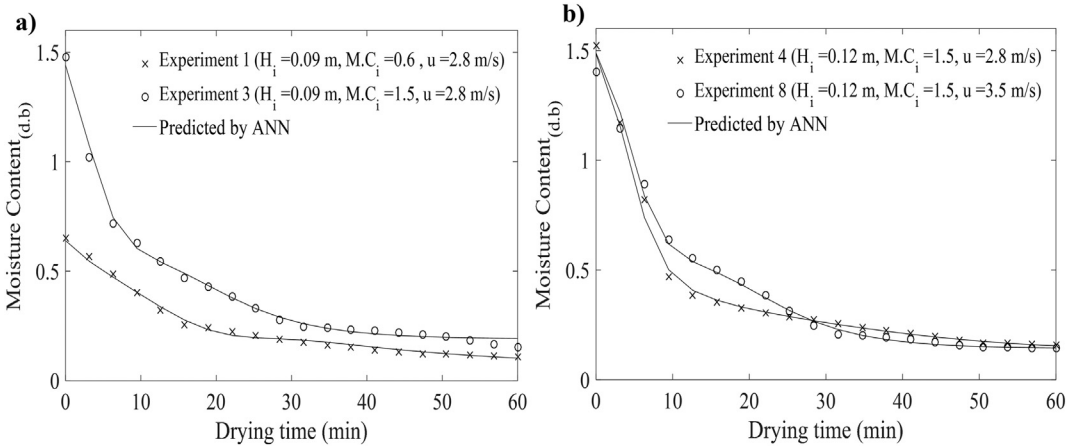

Fig. 9. Experimental and simulated variation of the moisture content: a) Run 1 (H_i = 0.09 m, $M.C_i$ = 0.6 e u_{air} = 2.8 m.s^{-1}) and Run 3 (H_i = 0.09 m, $M.C_i$ = 1.5 e u_{air} = 2.8 m.s^{-1}) and b) Run 4 (H_i = 0.12 m, $M.C_i$ = 1.5 e u_{air} = 2.8 m.s^{-1}) and Run 8 (H_i = 0.12 m, $M.C_i$ = 1.5 e u_{air} = 3.5 m.s^{-1}).

The MSE (0.0048) and RMSE (0.069) values obtained by the ANN model proved the satisfactory efficiency of prediction performance for variation in the three physical properties of the pieces of guava studied following drying in the spouted bed. Figs. 7, 8 and 9 showed the experimental values for the physical properties, which are close to the values computed by the ANN model.

3.3. Heat and mass transfer analysis obtained through the hybrid model simulation

The effect of the guava piece property variation (density, diameter and moisture content) through the prediction made by the ANN model should be added to the phenomenological model in order to simulate the thermal and water content evolution of both phases in the spouted bed drier.

Fig. 10a and b show the simulated particle and outlet air temperature (°C) variation for different experimental conditions of H_i, $M.C_i$ and u_{air}.

In the first 50s, a rapid constant drying period associated with wet bulb temperature was expected for the particles and output air. It is shown in Figs. 10 (a) and (b) where the particle temperature drops to 23 °C for the experiments 1 and 2.

For the particle temperature variation presented in Fig. 10a and b, one can note that this temperature increases quickly until stabilisation

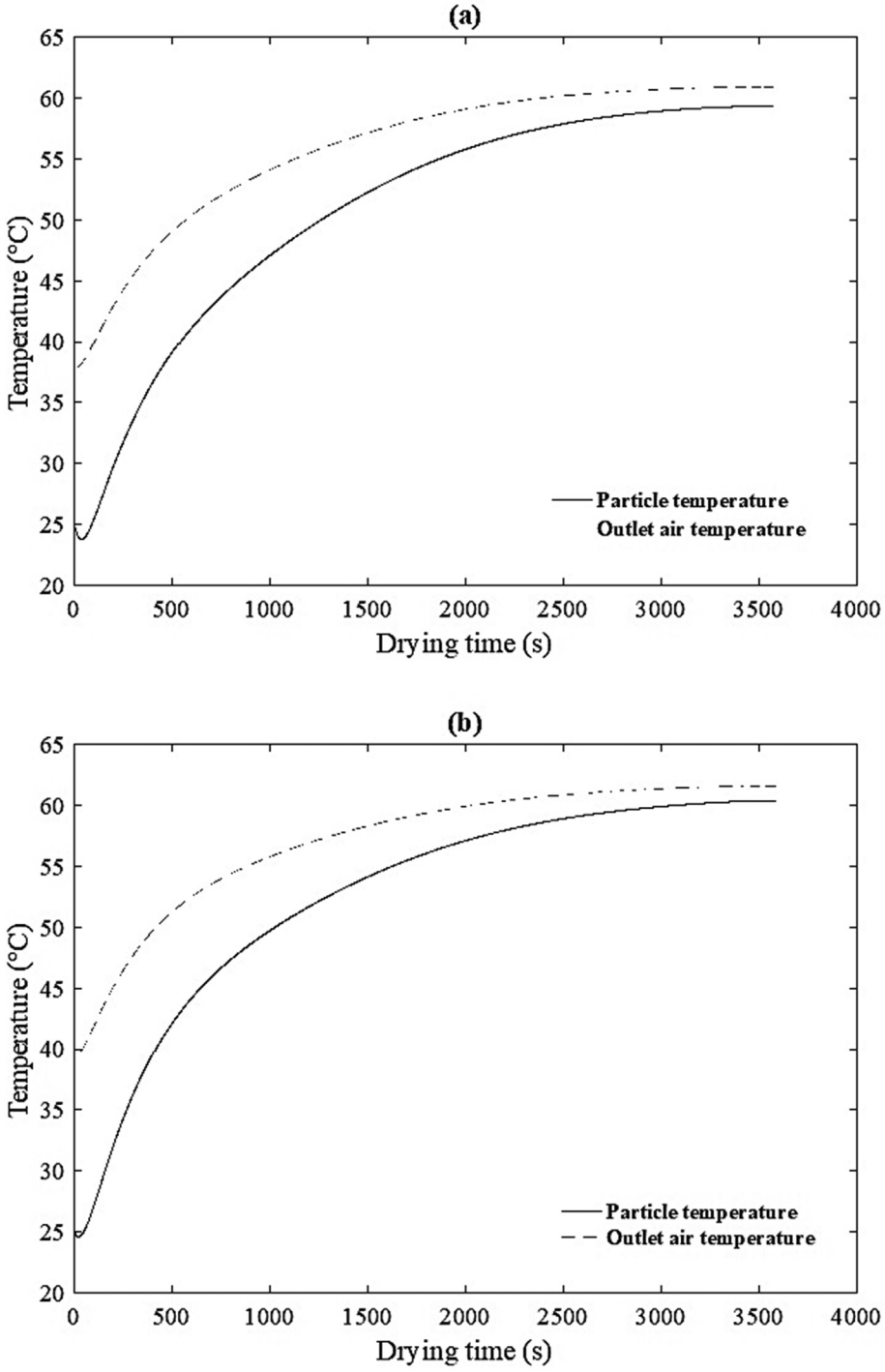

Fig. 10. Simulation of particle and outlet air temperature variation: a) Run 1 ($H_i = 0.09$ m, $M.C_i = 0.6$ and $u_{air} = 2.8\ m.s^{-1}$) and b) Run 2 ($H_i = 0.12$ m, $M.C_i = 0.6$ and $u_{air} = 2.8\ m.s^{-1}$).

at 2500 s. At this operation time, the particle temperature is 58 °C (experiment 1) and 59 °C (experiment 2), close to the inlet and stabilised air temperature (60 °C). This particle temperature behaviour is in accordance with the one observed in the falling rate drying period. As seen in these figures, the thermal equilibrium between air and particles is almost reached with a little temperature difference due to the heat lost to the ambient (Q_p), not significant at the studied conditions.

The simulated results of the outlet air humidity and the particle moisture content are presented in Fig. 11a and b under different experimental conditions.

The particle moisture content simulations (Fig. 11a and b) show the time required to evaporate most of the moisture presented in the pieces of guava is about 2500 s, coinciding with the time required for the particle temperature to reach thermal stabilisation, as can be seen in Fig. 10a and b. This behaviour is also observed in the simulation of barley drying [8]. This phenomenon occurs because the mass transfer in the particles is controlled by the diffusion mechanism coupled with the heat transfer and the particle temperature rises above the wet bulb temperature to stabilise at intermediate condition between the inlet and outlet of the air.

In Fig. 11a and b, experimental points of particle moisture content are included in order to validate the simulated results and a good agreement can be seen. Figs. 10 and 11 are simulated results based in the phenomenological predictions obtained through the ANN output parameters. Although only the particle moisture content are shown to validate the model with experimental data, in Fig. 11, the consistency of the other results allows us to admit its reliability.

The hybrid model methodology presented here was successfully applied to the specific case used to exemplify the use of the tool. It may be extended to other cases of spouted bed drying of deformable particles provided that experimental data of physical property variation kinetics were available to feed the database and that operating conditions are within the applicability range of the correlations used. In future work the model and the simulation program presented here will be expanded to improve the generality of its application through a user-friendly interface.

4. Conclusion

A hybrid model was developed for simulation of the drying of the guava pieces in a SB. The ANN model developed is able to estimate parameters for the resolution of the hybrid model (phenomenological/ ANN-PSO). In addition, the neural model can be used either alone to improve prediction quality of the end-product or coupled

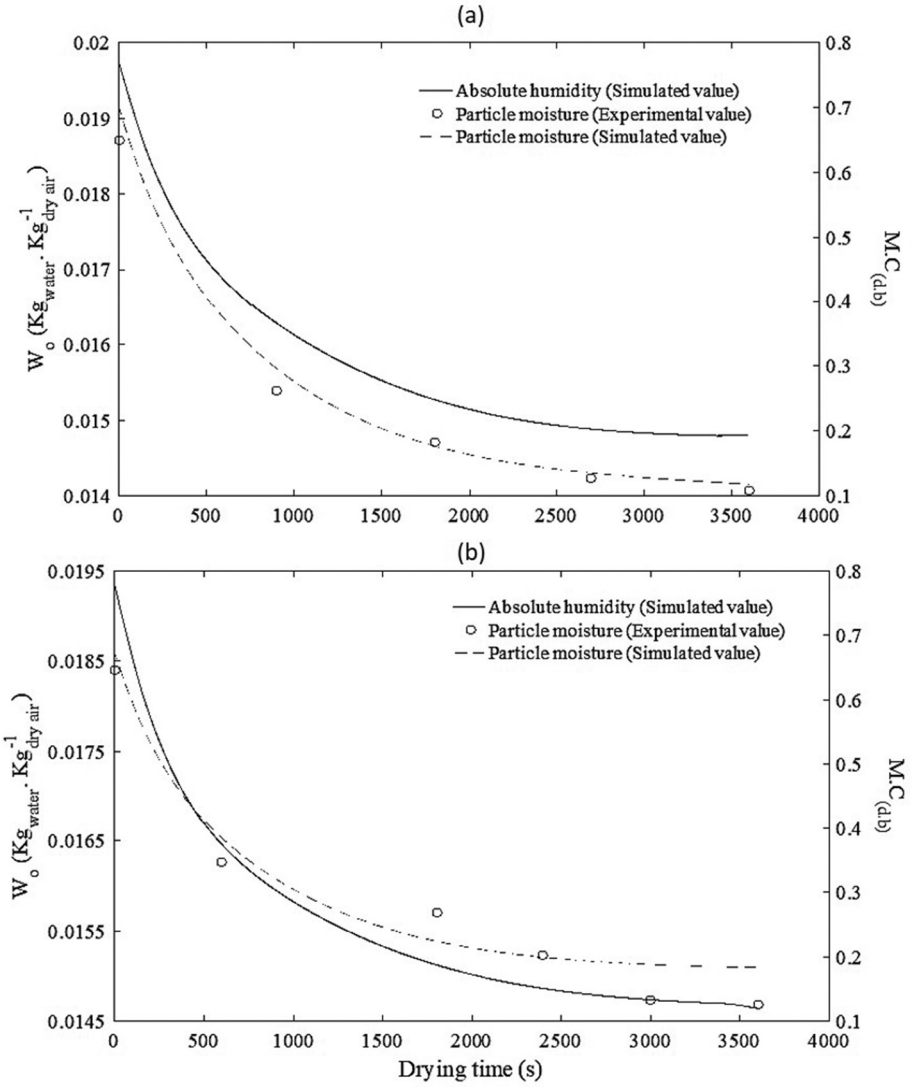

Fig. 11. Simulation of the absolute humidity of the air and moisture content of the particles: a) Run 1 ($H_i = 0.09$ m, $M.C_i = 0.6$ and $u_{air} = 2.8\ m.s^{-1}$) and b) Run 2 ($H_i = 0.12$ m, $M.C_i = 0.6$ and $u_{air} = 2.8\ m.s^{-1}$).

with phenomenological model to monitor and control the process in real-time. By controlling some operational variables of the SB dryer, such as air velocity, stable fluid dynamic regimes can be guaranteed independent of changes in the physical properties of the deformable material. Thus, the modelling technique using neural networks has shown promise for all drying applications of a similar nature to deformable solid particles e.g. fixed bed, fluidised bed and especially spouted bed dryer to predict stable operating conditions and control the flow instability. This research represents a first step to develop an intelligent and real-time control system due to the need to maintain the stable flow regime and rigid temperature control in order to avoid thermal degradation.

Declaration of Competing Interest

The authors declare that they have no known competing financial interests or personal relationships that could have appeared to influence the work reported in this paper.

Acknowledgement

This research was supported by CAPES (Coordination for the Improvement of Higher Education Personnel) under financing code 001, FAPITEC/SE (Foundation of Support to Research and Technological Innovation of the State of Sergipe) and CNPq (National Council for Scientific and Technological Development; grant number 420717/2018-8.

References

[1] I. Bialobrzewski, M. Zielinska, A. Mujundar, M. Markowski, Heat and mass transfer during drying of a bed of shrinking particles - simulation for carrot cubes dried in a spout-fluidised-bed drier, Int. J. Heat Mass Transf. 51 (2008) 4704–4716, https://doi.org/10.1016/j.ijheatmasstransfer.2008.02.031.

[2] M. Aghbashlo, S. Hosseinpour, A.S. Mujumdar, Application of artificial neural networks (ANNs) in drying technology: a comprehensive review, Dry. Technol. 33 (2015) 1397–1462, https://doi.org/10.1080/07373937.2015.1036288.

[3] H. Gao, X. Gong, G. Hu, Statistical and frequency analysis of pressure fluctuation in an annular spouted bed of coarse particles, Powder Technol. 317 (2017) 216–223, https://doi.org/10.1016/j.powtec.2004.02.003.

[4] H. Zhang, M. Liu, T. Li, Z. Huang, X. Sun, H. Bo, Y. Dong, Experimental investigation on gas-solid hydrodynamics of coarse particles in a two-dimensional spouted bed, Powder Technol. 307 (2017) 175–183, https://doi.org/10.1016/j.powtec.2016.11.024.

[5] S.C.S. Rocha, J.S. Souza, O.L.S. Alsina, M.F.D. Medeiros, Drying of tropical fruit pulps: spouted bed process optimisation as a function of pulp composition, Dry. Technol. 29 (2011) 1587–1599, https://doi.org/10.1080/07373937.2011.585442.

[6] J.T. Freire, F.B. Freire, M.C. Ferreira, B.S. Nascimento, A hybrid lumped parameter/neural network model for spouted bed drying of pastes with inert particles, Dry. Technol. 30 (2012) 1342–1353, https://doi.org/10.1080/07373937.2012.684085.

[7] S.B. Nascimento, F.B. Freire, J.T. Freire, Neuronal and grey modelling of Milk drying in spouted bed, Can. J. Chem. Eng. 91 (2013) 1815–1821, https://doi.org/10.1002/cjce.21886.

[8] P.T. Robbins, P.J. Fryer, The spouted-bed roasting of barley: development of a predictive model for moisture and temperature, J. Food Eng. 59 (2003) 199–208, https://doi.org/10.1016/S0260-8774(02)00459-4.

[9] L.N. Kahyaoglu, S. Sahin, G. Sumnu, Physical properties of parboiled wheat and bulgur produced using spouted bed and microwave assisted spouted bed drying, J. Food Eng. 98 (2010) 159–169, https://doi.org/10.1016/j.jfoodeng.2009.12.022.

[10] M.M. Almeida, O.S. Silva, O.L.S. Alsina, Fluid-dynamic study of deformable materials in spouted-bed dryer, Dry. Technol. 24 (2006) 499–508, https://doi.org/10.1080/07373930600612024.

[11] C.V. Bezerra, E.R. Amante, D.C. Oliveira, A.M.C. Rodigues, L.H.M. Silva, Green Banana (*Musa Cavendishii*) flour obtained in spouted bed - effect of drying on physicochemical, functional and morphological characteristics of the starch, Ind. Crop. Prod. 41 (2013) 241–249, https://doi.org/10.1016/j.indcrop.2012.04.035.

[12] G. Yousefi, Z. Emam-Djomeh, M. Omid, G.R. Askari, Prediction of physicochemical properties of raspberry dried by microwave-assisted fluidised bed dryer using artificial neural network, Dry. Technol. 32 (2014) 4–12, https://doi.org/10.1080/07373937.2013.801849.

[13] M. Zielinska, M. Markowski, Drying behavior of carrots dried in a spout–fluidised bed dryer, Dry. Technol. 25 (2007) 261–270, https://doi.org/10.1080/07373930601161138.

[14] G.F.M.V. Souza, R.F. Miranda, F.S. Lobato, M.A.S. Barrozo, Simultaneous heat and mass transfer in a fixed bed dryer, Appl. Therm. Eng. 90 (2015) 38–44, https://doi.org/10.1016/j.applthermaleng.2015.06.088.

[15] C. Niamnuy, S. Devahastin, S. Soponronnarit, G.S. Vijaya Raghavan, Modeling coupled transport phenomena and mechanical deformation of shrimp during drying in a jet spouted bed dryer, Chem. Eng. Sci. 63 (2008) 5503–5512, https://doi.org/10.1016/j.ces.2008.07.031.

[16] M.S. Leite, B.F. Santos, L.M.F. Lona, F.V. Silva, A.M.F. Fileti, Application of artificial intelligence techniques for temperature prediction in a polymerisation process, Chem. Eng. Trans. 24 (2011) 385–390, https://doi.org/10.3303/CET1124065.

[17] B. Santos, M. Leite, F. Silva, A. Fileti, Neural network model predictive control of a styrene polymerisation plant: online testing using an electronic worksheet, Chem. Pap. 66 (2012) 654–663, https://doi.org/10.2478/s11696-012-0165-z.

[18] S. Sunphorka, B. Chalermsinsuwan, P. Piumsomboon, Artificial neural network model for the prediction of kinetic parameters of biomass pyrolysis from its constituents, Fuel 193 (2017) 142–158, https://doi.org/10.1016/j.fuel.2016.12.046.

[19] D.F. Viana, G.R. Salazar-banda, M.S. Leite, Electrochemical degradation of reactive black 5 with surface response and artificial neural networks optimisation models, Sep. Sci. Technol. 00 (2018) 1–15, https://doi.org/10.1080/01496395.2018.1463264.

[20] Y.M.S. Veloso, M.M. Almeida, O.L.S. Alsina, M.S. Leite, Artificial neural network model for the flow regime recognition in the drying of guava pieces in the spouted bed, Chem. Eng. Commun. (2019) 1–10, https://doi.org/10.1080/00986445.2019.1608192.

[21] C. Wang, Z. Zhong, E. Jiaqiang, Flow regime recognition in spouted bed based on recurrence plot method, Powder Technol. 219 (2012) 20–28, https://doi.org/10.1016/j.powtec.2011.11.051.

[22] C. Wang, Z. Zhong, R. Li, Flow Regime recognition in the spouted bed based on Hilbert-Huang transformation, Korean J. Chem. Eng. 28 (2011) 308–313, https://doi.org/10.1007/s11814-010-0341-1.

[23] T. Mihajlovic, S. Ibric, A. Mladenovic, Application of design of experiments and multilayer perceptron neural network in optimisation of the spray-drying process, Dry. Technol. 29 (2011) 1638–1647, https://doi.org/10.1080/07373937.2011.592960.

[24] B.G. Silva, A.M.F. Fileti, O.P. Taranto, Drying of Brazilian pepper-tree fruits (*Schinus Terebinthifolius* Raddi): development of classical models and artificial neural network approach, Chem. Eng. Commun. 202 (2015) 1089–1097, https://doi.org/10.1080/00986445.2014.901220.

[25] K. Ameer, S.W. Bae, Y. Jo, H.G. Lee, A. Ameer, J.H. Kwon, Optimisation of microwave-assisted extraction of Total extract, Stevioside and Rebaudioside-a from stevia Rebaudiana (Bertoni) leaves, using response surface methodology (RSM) and artificial neural network (ANN) modelling, Food Chem. 229 (2017) 198–207, https://doi.org/10.1016/j.foodchem.2017.01.121.

[26] A.B. Silva Costa, F.B. Freire, J.T. Freire, M.C. Ferreira, Modelling drying pastes in vibrofluidised bed with inert particles, Chem. Eng. Process. Process Intensif. 103 (2016) 1–11, https://doi.org/10.1016/j.cep.2015.09.012.

[27] D. Geldart, Types of gas fluidisation, Powder Technol. 7 (1973) 285–292, https://doi.org/10.1016/0032-5910(73)80037-3.

[28] A.M. Ghahdarijani, F. Hormozi, A.H. Asl, Convective heat transfer and pressure drop study on Nanofluids in double-walled reactor by developing an optimal multilayer perceptron artificial neural network, Int. Commun. Heat Mass Transf. 84 (2017) 11–19, https://doi.org/10.1016/j.icheatmasstransfer.2017.03.014.

[29] P. Karthic, S. Joseph, N. Arun, S. Kumaravel, Optimisation of biohydrogen production by *Enterobacter* species using artificial neural network and response surface methodology, J. Renew. Sustain. Energy 5 (2013) 033104, https://doi.org/10.1063/1.4803746.

[30] N.G. Turan, O. Ozgonenel, Artificial neural network (ANN) approach for modelling Zn (II) adsorption from leachate using a new biosorbent, Chem. Eng. J. 173 (2011) 98–105, https://doi.org/10.1016/j.cej.2011.07.042.

[31] G.R. Oliveira, A.V. Santos, A.S. Lima, C.M.F. Soares, M.S. Leite, Neural modelling in adsorption column of cholesterol-removal efficiency from milk, LWT Food Sci. Technol. 64 (2015) 632–638, https://doi.org/10.1016/j.lwt.2015.05.051.

[32] G. Das, P.K. Pattnaik, S.K. Padhy, Artificial neural network trained by particle swarm optimisation for non-linear channel equalisation, Expert Syst. Appl. 41 (2014) 3491–3496, https://doi.org/10.1016/j.eswa.2013.10.053.

[33] M. Juneja, S.K. Nagar, Particle swarm optimisation algorithm and its parameters: a review, International Conference on Control, Computing, Communication and Materials (ICCCCM), IEEE, Oct, 2016.

[34] Q. Chang, H. Zhou, C. Hou, Using particle swarm optimisation algorithm in an artificial neural network to forecast the strength of paste filling material, J. China Univ. Min. Technol. 18 (2008) 0551–0555.

[35] M. Hassan, M. Hamada, Performance comparison of feed-forward neural networks trained with different learning algorithms for recommender systems, Computation 5 (2017) 40.

[36] L. Prechelt, Automatic early stopping using cross validation: quantifying the criteria, Neural Netw. 11 (1998) 761–767.

[37] R. Setiono, Feedforward neural network construction using cross validation, Neural Comput. 13 (2001) 2865–2877.
[38] O. Uemaki, M. Kugo, Heat transfer in spouted beds, Kagaku Kogaku *31* (1966) 348–453*N24*.
[39] A. Chatterjee, R.S.S. Adusumilli, A.V. Deshmukh, Wall-to-bed heat transfer characteristics of spout-fluid beds, Can. J. Chem. Eng. 61 (1983) 390–397, https://doi.org/10.1002/cjce.5450610320.
[40] S.W. Churchill, H.H.S. Chu, Correlating equations for laminar and turbulent free convection from a vertical plate, Int. J. Heat Mass Transf. 18 (1975) 1323–1329.
[41] F.A. Cubillos, E. Vyhmeister, G. Acuña, P.I. Alvarez, Rotary dryer control using a Grey-box neural model scheme, Dry. Technol. 29 (2011) 1820–1827, https://doi.org/10.1080/07373937.2011.604461.
[42] W. Zhong, X. Chen, J.R. Grace, N. Epstein, B. Jin, Intelligent prediction of minimum spouting velocity of spouted bed by back propagation neural network, Powder Technol. 247 (2013) 197–203, https://doi.org/10.1016/j.powtec.2013.07.022.
[43] G. Boracchi, L. Iliadis, C. Jayne, A. Likas, Engineering Applications of Neural Networks. 14th International Conference, Proceedings, Part I, EANN 2013, Halkidiki, Greece, September 2013 13–16.
[44] M.S. Hatamipour, D. Mowla, Shrinkage of carrots during drying in an inert medium fluidised bed, J. Food Eng. 55 (2002) 247–252, https://doi.org/10.1016/S0260-8774(02)00082-1.
[45] L. Mayor, A.M. Sereno, Modelling shrinkage during convective drying of food materials: a review, J. Food Eng. 61 (2004) 373–386, https://doi.org/10.1016/S0260-8774(03)00144-4.